http://dx.doi.org/10.5935/0103-5053.20150121

J. Braz. Chem. Soc., Vol. 26, No. 7, 1520-1526, 2015.
Printed in Brazil - ©2015 Sociedade Brasileira de Química
0103 - 5053 $6.00+0.00

Article

Surfactant-Assisted Preparation of FeCu Catalyst for Fischer-Tropsch Synthesis

Cailian Ma,[a,b] Yilong Chen[c] and Jiangang Chen[*,a]*

[a]*State Key Laboratory of Coal Conversion, Institute of Coal Chemistry, Chinese Academy of Sciences, 030001 Taiyuan, P. R. China*

[b]*University of Chinese Academy of Sciences, 100049 Beijing, P. R. China*

[c]*State Key Laboratory of Biomass Thermal Chemistry Technology, 430223 Wuhan, P. R. China*

FeCu catalysts were prepared by co-precipitation method with or without the assistance of the surfactant, polyvinyl pyrrolidone (PVP), polyvinyl alcohol (PVA) or polyethylene glycol (PEG). The effect of surfactant on the structure and catalytic behavior of FeCu catalysts was investigated. The catalysts were characterized by inductively coupled plasma (ICP) spectroscopy, Brunauer-Emmett-Teller (BET) surface area, scanning electron microscopy (SEM), transmission electron microscopy (TEM), X-ray diffraction (XRD), H_2-temperature-programmed reduction (TPR) and Fourier transform infrared (FTIR) spectroscopy techniques. They were tested for Fischer-Tropsch synthesis (FTS) at 230-310 °C. The results showed that the catalysts prepared with PVA were more active than the catalysts prepared without any surfactant's assistance, the catalysts prepared with PVP and the catalysts prepared with PEG. In addition, the morphologies of the iron catalysts can be controlled by different surfactants. Meanwhile, addition of surfactant remarkably influenced the growth orientation of hematite nanocrystals, resulting in preferential exposure of the (110) plane. The characterization results revealed that PVA can promote the dispersion of iron oxides and the formation of the more active phase on the catalyst.

Keywords: Fischer-Tropsch synthesis, FeCu catalyst, co-precipitation method, surfactant

Introduction

The Fischer-Tropsch (FT) reaction is a heterogeneous catalytic reaction that converts synthesis gas, that is, a mixture of carbon monoxide (CO) and hydrogen (H_2), into mainly linear hydrocarbons.[1,2] Iron-based catalyst is favored due to its low cost, adjustable selectivity, and reasonable water-gas shift (WGS) activity, which means a flexible operation for the industrial process.[3-5]

Transition metal promoter, such as Cu, is also incorporated into iron-based Fischer-Tropsch synthesis (FTS) catalyst to optimize the chemical environment of the catalyst. Among them, Cu is widely used in commercial FTS process, because the presence of Cu facilitates the reduction of α-Fe_2O_3 to Fe_3O_4 or metallic Fe.[6,7]

Generally, the preparation method of catalysts is one of the fundamental factors that play an important role in the precursor structure of catalysts and in the activity of catalysts.[8-10] Co-precipitation method has been used in the preparation of iron-based catalysts.[11-13] However, difficulties in controlling both the particle size and the crystal phases are the main drawbacks of this method. In addition, the FT reaction is a structure sensitive reaction.[14] A well-known method for the preparation of porous nanostructures is the surfactant-template method combined with a conventional synthesis route such as the co-precipitation. The surfactants have been already demonstrated as powerful agents to control the size and shape of nanomaterials (both inorganic and organic) because of the strong interaction between surfactants and crystal surfaces during the formation of nanocrystals.[15] When surfactants are used as reaction media, surfactants are capable to control the growth of bulky crystals. Nowadays, different surfactants have shown potential applications in many fields such as catalysis,[16] electrochemistry,[17] and so on.[18-20] Luo *et al.*[16] investigated that high-surface area nanosized CuO-CeO_2 catalysts were prepared by a surfactant-templated method and showed high catalytic activity for selective oxidation of CO. In addition, Li and co-workers[17] found that cobalt nickel double hydroxides nanoparticles were synthesized by a polyvinyl pyrrolidone-assisted chemical co-precipitation method and the $Co_{0.57}Ni_{0.43}$ LDH electrode

*e-mail: chenjg19@163.com

also demonstrated a good cycling performance. Thus, the addition of the surfactant in catalyst is essential. However, little research on their applications in FTS has been done. Based on this, the effect of different surfactants on the performance of Fischer-Tropsch synthesis over FeCu catalysts were investigated in the present study.

A series of FeCu catalysts were prepared by co-precipitation method with or without the assistance of the surfactant, polyvinyl pyrrolidone (PVP), polyvinyl alcohol (PVA) or polyethylene glycol (PEG). These catalysts were characterized by inductively coupled plasma (ICP) spectroscopy, Brunauer-Emmett-Teller (BET) surface area, scanning electron microscopy (SEM), transmission electron microscopy (TEM), X-ray diffraction (XRD), H_2-temperature-programmed reduction (TPR) and Fourier transform infrared (FTIR) spectroscopy techniques. The performance of Fischer-Tropsch synthesis over the catalysts was investigated. The relation between the structure and the catalytic activity of these catalysts in Fischer-Tropsch synthesis was also discussed.

Experimental

Catalyst preparation

FeCu catalysts, with the mass ratio of Fe/Cu = 100:6, were prepared by co-precipitation method with or without the assistance of surfactant. For a typical synthesis, 30 mmol $Fe(NO_3)_3$ and 1.59 mmol $Cu(NO_3)_2$ were added into a solution with or without the surfactant, PVP, PVA or PEG at room temperature under constant stirring. After the mixture was stirred for 0.5 h, ammonia solution (20 wt.%) was added into the solution and the pH was maintained at 8.5. The obtained precipitate was aged for 2 h at room temperature, and then washed and filtered. After that, the filtered cakes were dried at 100 °C for 6 h, followed by calcination at 500 °C for 6 h in air. In this study, the FeCu catalysts, prepared with no surfactant, 15 wt.% of PVP, 15 wt.% of PVA and 15 wt.% of PEG, were denoted as FeCu-Blank, FeCu-PVP, FeCu-PVA and FeCu-PEG, respectively. Table 1 shows the physical properties of precipitated iron catalysts.

Characterization

The physico-chemical characteristics of catalysts were characterized by ICP, BET, XRD, SEM, TEM, H_2-TPR and FTIR techniques.

The actual composition of the catalysts was determined by ICP-atomic emission spectroscopy (AES). To prepare the solution for elemental analysis, 2 mL of concentrated nitric acid was used to dissolve 40 mg of catalyst sample, followed by adding 2 mL of 30 wt.% H_2O_2; the solution was then diluted to 1000 mL with deionized water.

BET surface area of the catalysts was measured by nitrogen sorption at –195.8 °C with a TriStar 3000 Gas Absorption Analyzer. The pore diameter was calculated by applying the Barrett-Joyner-Halenda method (BJH) to the adsorption branches of the N_2 isotherms. The samples were degassed at 200 °C and 6.7 Pa for 2 h prior to the measurement.

The morphology of catalysts was investigated by SEM (Jeol JSM-6701F). The catalysts were treated by desiccation and spray-gold.

TEM images of the catalysts were obtained by using a Jeol JEM 2010 microscope operating at 200 kV. The catalysts were dispersed in ethanol and mounted on a carbon foil supported on a copper grid.

XRD measurements were carried out with a D/max-RA X-ray diffractometer (Rigaku), equipped with Cu Kα radiation (λ = 1.5406 Å) at 40 kV and 150 mA. The measurements were made at room temperature in the 2θ range of 10-80 °C with a scanning rate of 2 or 4° min^{-1}.

H_2-TPR experiment was performed in a conventional atmospheric quartz reactor (5 mm i.d.). A flow of 5% H_2/95% Ar (v/v), maintained at a flow of 50 mL min^{-1}, was used as the reduction gas, and the TPR profiles were recorded by using the response of the thermal conductivity detector (TCD) of the effluent gas. Typically, 50 mg samples were loaded and reduced by 5% H_2/95% Ar (v/v) with the temperature rising from room temperature to 1000 °C at a rate of 10 °C min^{-1}.

FTIR spectra were recorded in the 400-4000 cm^{-1} range with a Bruker Vertex 70 FTIR, using the KBr pellet technique.

Table 1. Physical properties of precipitated iron catalysts

Catalyst	Mass of catalyst / g	Component (on mass basis) analyzed		BET result		
		Fe	Cu	Surface area / (m^2 g^{-1})	Pore volume / (cm^3 g^{-1})	Average pore size / nm
FeCu-Blank	2.33	100	5.8	24.02	0.088	14.68
FeCu-PVP	1.45	100	5.8	12.65	0.055	17.51
FeCu-PVA	1.02	100	5.7	7.78	0.037	19.36
FeCu-PEG	1.25	100	5.9	2.73	0.016	24.25

Catalytic activity

The FTS performance of the catalysts was tested in a stainless steel fixed-bed reactor with inner diameter of 12 mm. A volume of 2 mL of catalyst was loaded into the reactor for all the reaction tests, and the mass of catalyst is listed in Table 1. The remaining volume of the reactor tube was filled with quartz granules. All the catalysts were activated with syngas (H_2/CO = 2.0) at 280 °C, 0.30 MPa, and 1000 h^{-1} for 24 h. The reaction conditions were maintained at 1.5 MPa, 2000 h^{-1}, and H_2/CO = 2.0. A detailed description of the reactor and product analysis systems has been given elsewhere.[21]

Results and Discussion

Textural properties of catalysts

The textual properties of the calcined catalysts prepared with or without the assistance of different surfactants are shown in Table 1 and Figure 1. It can be seen that the BET surface area of catalyst prepared with no surfactant (FeCu-Blank) is about 24 $m^2 g^{-1}$. Much smaller BET surface area and total pore volume are found for the catalysts prepared with surfactant compared with the catalyst prepared with no surfactant (FeCu-Blank), especially for FeCu-PEG catalyst. In addition, the average pore diameter of the catalysts prepared with surfactant is higher than that of FeCu-Blank catalyst. The pore size distribution (PSD) in Figure 1 shows a smaller pore diameter (4-15 nm) in the FeCu-Blank catalyst. For the catalysts prepared with surfactant, the PSD curve shifts to higher pore diameter compared with the FeCu-Blank catalyst, especially for FeCu-PEG catalyst. It indicates that with the introduction of the surfactant in the course of preparing the binary matrix, the BET surface area of catalysts becomes small and pore diameter of catalysts becomes large, due to the interaction between catalyst precursors and surfactant.[20] It is well known that non-ionic surfactant can be adsorbed on particles in the form of surface micelles (or bilayer-like structures) and provide stereo repulsion during Brownian collisions, even in the absence of electrostatic repulsive forces.[22]

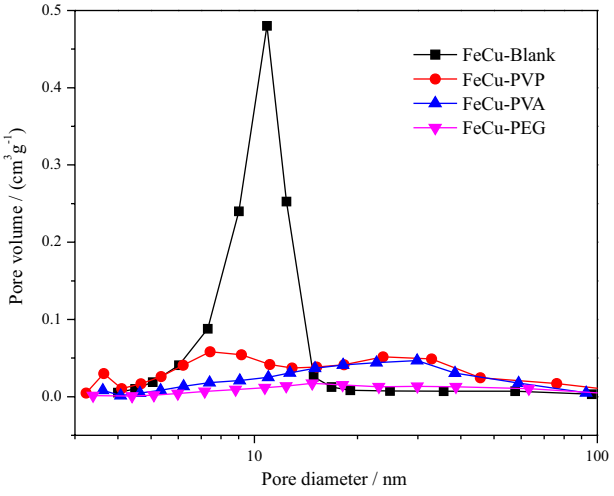

Figure 1. Pore size distribution of the calcined catalysts.

Morphology of catalysts

The morphology and structural details of the catalyst were examined using SEM and TEM, as shown in Figures 2 and 3, respectively. FeCu-Blank catalyst has a relatively loose morphology mainly consisting of spherical aggregates (Figures 2a and 3a) at particle diameter of around 23 nm (Figure 3a, inset). FeCu-PVP catalyst is irregular bulk (Figure 2b). However, FeCu-PEG catalyst has a dense morphology composed of numerous irregular iron oxide particles (Figure 2d). Meanwhile, for the FeCu-PVA catalyst, the loose morphology exhibits highly porous structure (Figures 2c and 3b). In high magnification (Figure 2c, inset), nanoparticles of the FeCu-PVA catalyst arrange at random and form a loosely packed microstructure in the morphology requirement for easy gas diffusion and mass transport during FTS reaction. It indicates that the morphologies of the iron catalysts can be controlled by different surfactants.

Crystallite structure of catalysts

XRD patterns of the calcined catalysts prepared with or without the assistance of different surfactants are

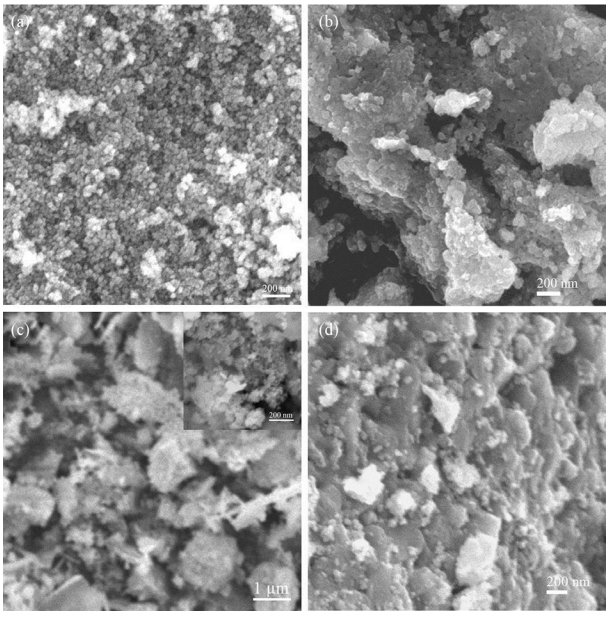

Figure 2. SEM images of the calcined catalysts: (a) FeCu-Blank; (b) FeCu-PVP; (c) FeCu-PVA and (d) FeCu-PEG.

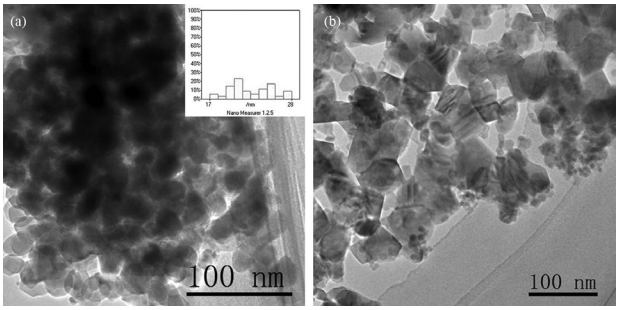

Figure 3. TEM images of the calcined catalysts: (a) FeCu-Blank and (b) FeCu-PVA.

presented in Figure 4a. The only detectable phase in the diffraction patterns of all catalysts is well-crystallized hematite (α-Fe_2O_3) with characteristic diffraction peaks at 2θ angles of 24.2, 33.1, 35.6, 40.8, 49.52, 54.0, 57.6, 62.5 and 64.0°.[23] Moreover, it can be found that the intensity of α-Fe_2O_3 characteristic peak increases in the order of FeCu-Blank < FeCu-PVP < FeCu-PVA < FeCu-PEG. It implies that the adding of surfactant in the preparation of iron catalyst promotes the growth of α-Fe_2O_3 crystallite. Interestingly, compared with the standard stick pattern (Joint Committee on Powder Diffraction Standards (JCPDS) Card No. 033-0664) of pure hematite, the peak of the (110) plane is anomalously higher than that of the (104) plane. This result indicates that the adding of surfactant in the preparation of iron catalyst remarkably influences the growth orientation of hematite nanocrystals, resulting in the preferential exposure of the (110) plane.

After reduction, all the peaks in the XRD pattern shown in Figure 4b can be indexed as the iron carbide (χ-Fe_5C_2) phase, with no other phase being detected, which is consistent with the previous reports.[24] The intensity of χ-Fe_5C_2 characteristic peak of FeCu-PVA is stronger than that of FeCu-PEG, FeCu-PVP and FeCu-Blank. The result demonstrates that the addition of PVA in the preparation of iron catalyst promotes the carburization of iron oxides. Iron carbide is the active phase for FTS.[13] All of the hematite in catalysts were reduced and rapidly transformed into active sites during reduction. As the reduction by syngas proceeded, iron oxide was transformed from $Fe_2O_3 \rightarrow Fe_3O_4 \rightarrow \alpha$-Fe or iron carbide. α-Fe could not be observed in our catalyst after reduction, because the metallic iron was fairly reactive to carbon dissociated from carbon monoxide.[24]

After reaction, the XRD patterns of the used catalysts are shown in Figure 4c. There are a few lines assigned to dilute quartz in all catalysts. There are several diffraction peaks at 35.5, 43.1, 57.0 and 62.6° along with the characteristic peaks of magnetite (Fe_3O_4) in the XRD patterns. Due to the poor crystallographic form of iron carbide, the peaks around 31 and 44.5° are broad, and it is impossible to identify which

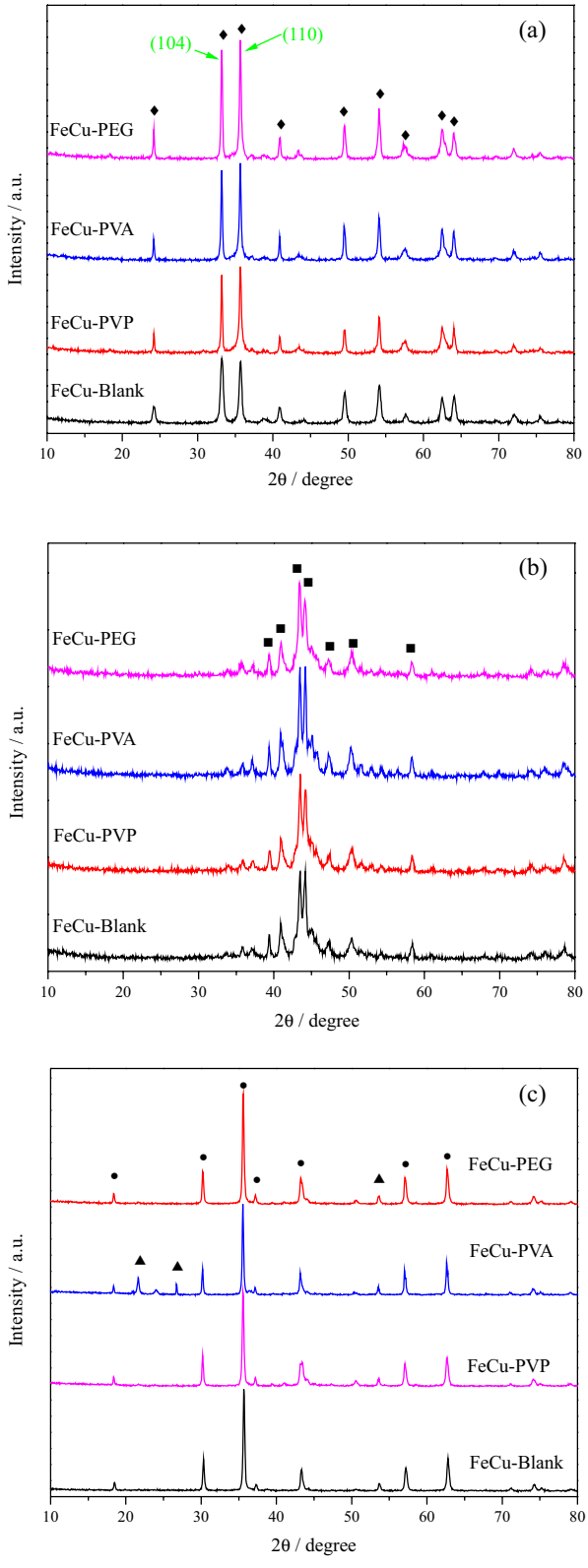

Figure 4. XRD pattern of catalysts (a) after calcination, (b) after reduction and (c) after reaction: (◆) hematite; (■) iron carbide; (●) magnetite; (▲) quartz.

carbide is present in the XRD patterns, or to determine the stoichiometry of this carbide from the XRD patterns.[25]

Nevertheless, the intensity of Fe_3O_4 characteristic peak increases in the order of FeCu-PVA < FeCu-Blank < FeCu-PVP < FeCu-PEG, so it can be concluded that more active phase were generated with addition of PVA in the course of preparing the binary matrix, which can also account for better catalytic performance over FeCu-PVA catalyst in Fischer-Tropsch synthesis. Davis and co-workers[26] and Datye and co-workers[27] reported that Fe_3O_4 was the only phase in iron catalysts after reaction detectable by XRD analysis, because of the poor crystallographic form of iron carbide.

Reduction behavior of catalysts

Figure 5 shows the H_2-TPR profiles of the calcined catalysts. It is obvious that there are two multiple hydrogen consumption peaks at different temperature range for all the catalysts. The low temperature (LT) reduction peaks are assigned to the transformations of CuO → Cu and Fe_2O_3 → Fe_3O_4, and the high temperature (HT) reduction peaks are due to the transformation of Fe_3O_4 → Fe.[28] Compared with the base FeCu-Blank, obvious delay of the reduction steps in the LT peaks can be observed for FeCu-PEG, FeCu-PVP and FeCu-PVA, especially for the FeCu-PEG catalyst. This indicates that with the introduction of surfactant in the course of preparing the binary matrix, the reduction temperature of resultant catalyst shifts to higher temperature related to the interaction between CuO and Fe_2O_3 lattices in FeCu catalyst.[28] Furthermore, all the catalysts show that the first peak can be split into three peaks, assigned to reduction of different phases. The first peak can be attributed to the reduction process of CuO → Cu. The second and third peaks can be attributed to the reduction of Fe_2O_3 → Fe_3O_4.[29] Notably, the LT reduction peaks became symmetrical with addition of different surfactants in the preparation of catalyst, suggesting a stronger interaction force formed with assistance of the surfactant.[15]

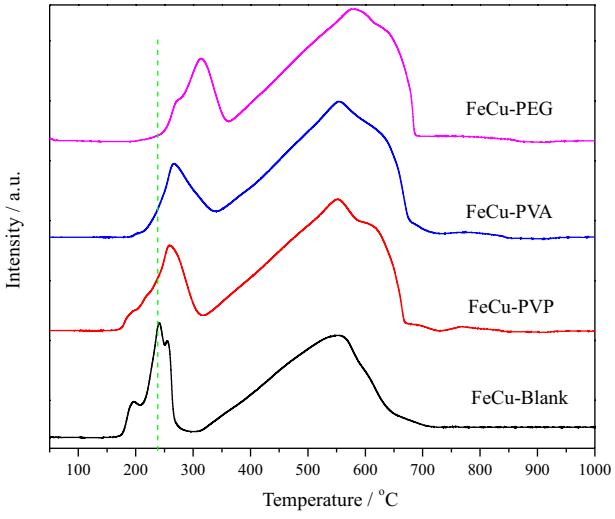

Figure 5. H_2-TPR profiles of catalysts.

FTIR of catalysts

As an organic assistant agent used during the preparation of the iron catalysts, FTIR is performed to examine whether the organic species is completely removed by later calcination pretreatment at 500 °C. The FTIR results of the catalysts are shown in Figure 6. The vibrational bands attributed to the crystallization water molecules and the constitution water molecules are observed in the ranges of 3600-3200 and 1700-1550 cm^{-1}, respectively.[30] In addition, the about 555 cm^{-1} band is attributed to the Fe–O stretching vibration.[31] From the spectra in Figure 6, it can be found that the bands of catalysts prepared with different surfactants are the same. This result suggests that the organic assistant agent can be completely removed through the calcination at 500 °C.[32]

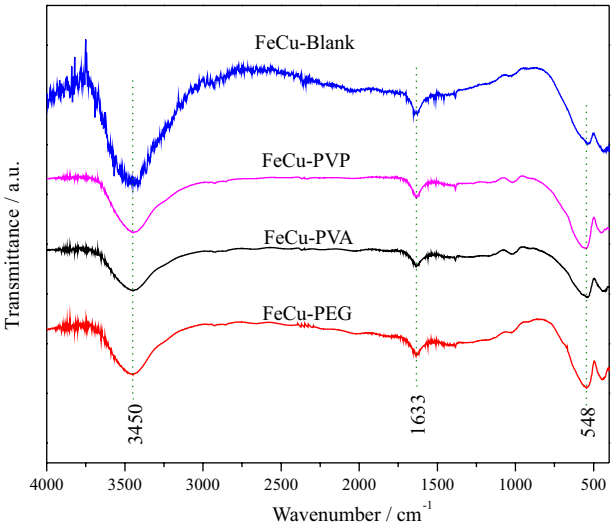

Figure 6. FTIR profiles of catalysts.

FTS performance

The catalytic activities of catalysts were characterized in a fixed bed reactor, as presented in Table 2. Figure 7 displays CO conversion as a function of temperature for the catalysts prepared with the assistance of different surfactants. The FeCu-PVA catalyst exhibits the markedly highest activity in all catalysts, while the activity of FeCu-PEG catalyst is lowest. Previous studies have shown that iron carbide is the active phase for FTS reaction[13] and formation of more iron carbide can increase activity of iron catalyst. Furthermore, the adding of PVA in catalyst

Table 2. Activity and selectivity of catalysts

Catalyst[a,b]	FeCu-Blank		FeCu-PVP		FeCu-PVA		FeCu-PEG	
Temperature / °C	240	300	240	300	240	300	240	300
TOF[c] × 10^{-3} / s^{-1}	0.42	1.19	0.75	1.63	1.92	3.03	0.50	1.89
CO conversion / %	22.42	62.75	24.76	55.88	44.39	70.09	14.45	55.09
CO + H_2 conversion / %	20.57	50.04	22.73	44.63	36.99	56.82	14.34	45.43
H_2 conversion / %	19.74	44.36	21.82	39.81	33.66	50.84	14.29	41.25
H_2/CO in tail gas	2.31	3.34	2.32	3.18	2.65	3.65	2.33	3.02
H_2/CO usage	1.97	1.58	1.97	1.66	1.69	1.61	2.31	1.73
K_{WGS}	0.99	2.33	0.84	1.78	1.28	2.01	1.60	1.81
CO_2 percent / mol%	11.92	27.34	11.07	22.37	17.25	22.84	18.61	20.80
HC[b] selectivity / wt.%								
C_1	17.27	29.90	16.11	29.11	9.80	26.03	19.23	30.91
C_{2-4}	43.21	54.31	43.13	55.23	32.14	54.77	47.05	58.04
C_5^+	39.52	15.79	40.76	15.66	58.06	19.19	33.72	11.05
C_{2-4} O/P	0.39	0.40	0.71	0.73	1.28	1.07	0.58	0.46
Alcohols[d] / wt.%	3.01	1.05	3.15	1.05	7.56	1.35	1.59	0.62

[a]Reaction condition: 1.5 MPa, H_2/CO = 2.0, and gas hourly space velocity (GHSV) = 2000 h^{-1}; [b]max error = ±5%; [c]apparent turnover frequency: numbers of CO molecules converted *per* adsorption site *per* second; [d]alcohols in total hydrocarbon and oxygenates. K_{WGS}: Water-gas shift activity.

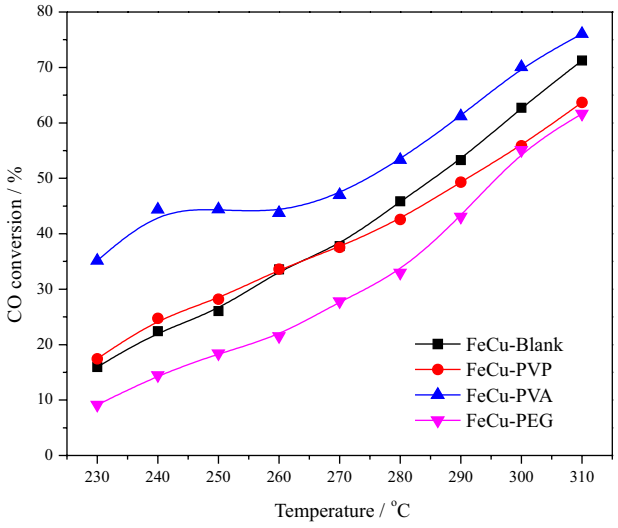

Figure 7. CO conversion as a function of temperature for catalysts.

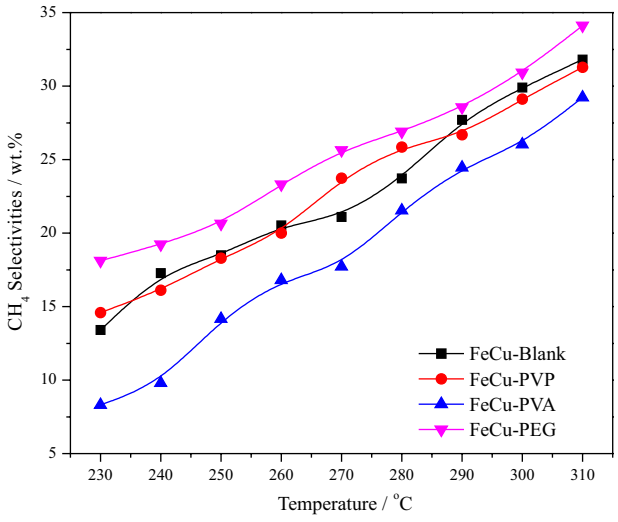

Figure 8. CH_4 selectivity as a function of temperature for catalysts.

preparation favors highly porous structure formation, which allows for easy gas diffusion and mass transport, and leads to increased CO conversion. The iron catalysts mainly produce hydrocarbons. The selectivity of methane over FeCu-PVA catalyst is inferior to that of other catalysts, as shown in Figure 8. In addition, selectivity of methane over FeCu-PEG catalyst is highest. Methane and C_2-C_4 are the main components in the hydrocarbon products due to the high reaction temperature, whilst the selectivity of C_5^+ over the iron catalysts is lower. FeCu-PVA catalyst also shows a much higher C_5^+ selectivity for FTS reaction than other catalysts, especially for FeCu-PEG, as shown in Figure 9. It can be found that the addition of PVA in catalyst preparation can improve the FTS performance of catalyst, but the addition of PEG in catalyst preparation suppresses the FTS performance of catalyst, which is in good agreement with the above characterization results.

Conclusions

A series of FeCu catalysts were prepared by co-precipitation method with or without the assistance of the surfactant, polyvinyl pyrrolidone (PVP), polyvinyl alcohol (PVA) or polyethylene glycol (PEG) in this paper. The FTS

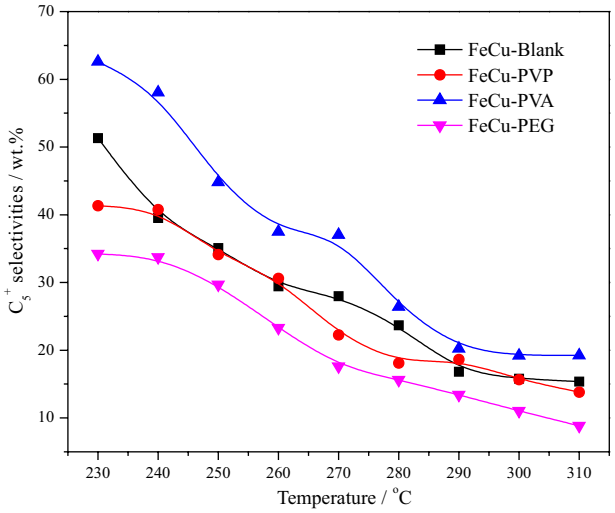

Figure 9. C_5^+ selectivity as a function of temperature for catalysts.

performance was investigated over the FeCu catalysts. The results showed that the FeCu-PVA catalyst prepared with PVA exhibited the most excellent FTS activity among all the catalysts investigated. Its superior FTS activity was favorable to formation of a loosely packed microstructure and the more iron carbide on the catalyst.

Acknowledgements

The authors are indebted to the support from the National Natural Science Foundation of China (No. 21373254). This work is also supported by Wuhan Kaidi General Research Institute of Engineering & Technology Co., Ltd.

References

1. Markvoort, A. J.; van Santen, R. A.; Hilbers, P. A. J.; Hensen, E. J. M.; *Angew. Chem., Int. Ed.* **2012**, *51*, 9015.
2. Bukur, D. B.; Lang, X.; *Ind. Eng. Chem. Res.* **1999**, *38*, 3270.
3. Wang, H. L.; Yang, Y.; Xu, J.; Wang, H.; Ding, M. Y.; Li, Y. W.; *J. Mol. Catal. A: Chem.* **2010**, *326*, 29.
4. Karn, F. S.; Seligman, B.; Shultz, J. F.; Anderson, R. B.; *J. Phys. Chem.* **1958**, *62*, 1039.
5. Diffenbach, R. A.; Fauth, D. J.; *J. Catal.* **1986**, *106*, 466.
6. Li, S.; Krishnamoorthy, S.; Li, A.; Meitzner, G. D.; Iglesia, E.; *J. Catal.* **2002**, *206*, 202.
7. Jin, Y.; Datye, A. K.; *J. Catal.* **2000**, *196*, 8.
8. Pawelec, B.; Halachev, T.; Olivas, A.; Zepeda, T.; *Appl. Catal., A* **2008**, *348*, 30.
9. Maity, S. K.; Flores, G. A.; Ancheyta, J.; Rana, M. S.; *Catal. Today* **2008**, *130*, 374.
10. Okamoto, Y.; Ishihara, S.-Y.; Kawano, M.; Satoh, M.; Kubota, T.; *J. Catal.* **2003**, *217*, 12.
11. Bukur, D. B.; Nowicki, L.; Manne, R. K.; Lang, X.; *J. Catal.* **1995**, *155*, 366.
12. Cui, X. J.; Xu, J.; Zhang, C. H.; Yang, Y.; Gao, P.; Wu, B. S.; Li, Y. W.; *J. Catal.* **2011**, *282*, 35.
13. Dry, M. E.; *Appl. Catal., A* **1996**, *138*, 319.
14. Boudart, M.; McDonald, M. A.; *J. Phys. Chem.* **1984**, *88*, 2185.
15. Liu, Y.; Goebl, J.; Yin, Y.; *Chem. Soc. Rev.* **2013**, *42*, 2610.
16. Luo, M. F.; Ma, J. M.; Lu, J. Q.; Song, Y. P.; Wang, Y. J.; *J. Catal.* **2007**, *246*, 52.
17. Xie, L. J.; Hu, Z. G.; Lv, C. X.; Sun, G. H.; Wang, J. L.; Li, Y. Q.; He, H. W.; Wang, J.; Li, K. X.; *Electrochim. Acta* **2012**, *78*, 205.
18. Gao, J. K.; Ye, K. Q.; Yang, L.; Xiong, W. W.; Ye, L.; Wang, Y.; Zhang, Q. H.; *Inorg. Chem.* **2013**, *53*, 691.
19. Adachi-Pagano, M.; Forano, C.; Besse, J.-P.; *Chem. Commun.* **2000**, 91.
20. Mercier, L.; Pinnavaia, T. J.; *Chem. Mater.* **2000**, *12*, 188.
21. Sun, J. Q.; Zheng, S. K.; Zhang, K.; Song, D. C.; Liu, Y. T.; Sun, X. D.; Chen, J. G.; *J. Mater. Chem. A* **2014**, *2*, 13116.
22. Cellesi, F.; Tirelli, N.; *Colloids Surf., A* **2006**, *288*, 52.
23. Suo, H. Y.; Zhang, C. H.; Wu, B. S.; Xu, J.; Yang, Y.; Xiang, H. W.; Li, Y. W.; *Catal. Today* **2012**, *183*, 88.
24. Hayakawa, H.; Tanaka, H.; Fujimoto, K.; *Catal. Commun.* **2007**, *8*, 1820.
25. Yang, Y.; Xiang, H. W.; Xu, Y. Y.; Bai, L.; Li, Y. W.; *Appl. Catal., A* **2004**, *266*, 181.
26. Huang, C. S.; Xu, L.; Davis, B. H.; *Fuel Sci. Technol. Int.* **1993**, *11*, 639.
27. Shroff, M. D.; Kalakkad, D. S.; Coulter, K. E.; Kohler, S. D.; Harrington, M. S.; Jackson, N. B.; Sault, A. G.; Datye, A. K.; *J. Catal.* **1995**, *156*, 185.
28. Chu, Z.; Chen, H. B.; Yu, Y.; Wang, Q.; Fang, D. Y.; *J. Mater. Chem. A* **2013**, *366*, 48.
29. Suo, H. Y.; Wang, S.; Zhang, C. H.; Xu, J.; Wu, B. S.; Yang, Y.; Xiang, H. W.; Li, Y. W.; *J. Catal.* **2012**, *286*, 111.
30. Guo, F.; Guo, S.; Qiu, Z.; Zhao, L.; Xiang, H.; *J. Braz. Chem. Soc.* **2014**, *25*, 750.
31. Cozar, O.; Leopold, N.; Jelic, C.; Chiş, V.; David, L.; Mocanu, A.; Tomoaia-Cotişel, M.; *J. Mol. Struct.* **2006**, *788*, 1.
32. Li, S. N.; Zhu, H. F.; Qin, Z. F.; Wang, G. F.; Zhang, Y. G.; Wu, Z. W.; Li, Z. K.; Chen, G.; Dong, W. W.; Wu, Z. G.; *Appl. Catal., B* **2014**, *144*, 498.

Submitted: December 7, 2014
Published online: May 15, 2015